



UNIVERSIDAD DISTRITAL
FRANCISCO JOSÉ DE CALDAS



Research

Estimating Acceleration from a Single Uniform Linear Motion-Blurred Image using Homomorphic Mapping and Machine Learning

Estimación de la aceleración a partir de una única imagen borrosa de movimiento lineal uniforme utilizando el enfoque de mapeo homomórfico y aprendizaje automático

Jimmy Alexander Cortés-Osorio¹  , Juan Bernardo Gómez-Mendoza² , Juan Carlos Riaño-Rojas² 

¹Universidad Tecnológica de Pereira, Pereira, Risaralda, Colombia 

²Universidad Nacional de Colombia sede Manizales, Manizales, Caldas, Colombia 

Abstract

Context: Vision-based measurement (VBM) systems are becoming popular as an affordable and suitable alternative for scientific and engineering applications. When cameras are used as instruments, motion blur usually emerges as a recurrent and undesirable image degradation, which in fact contains kinematic information that is usually dismissed.

Method: This paper introduces an alternative approach to measure relative acceleration from a real invariant uniformly accelerated linear motion-blurred image. This is done by using homomorphic mapping to extract the characteristic Point Spread Function (PSF) of the blurred image, as well as machine learning regression. A total of 125 uniformly accelerated motion-blurred pictures were taken in a light- and distance-controlled environment, at five different accelerations ranging between 0,64 and 2,4 m/s². This study evaluated 19 variants such as tree ensembles, Gaussian processes (GPR), and linear, support vector machine (SVM), and tree regression.

Results: The best RMSE result corresponds to GPR (Matern 5/2), with 0,2547 m/s² and a prediction speed of 530 observations per second (obs/s). Additionally, some novel deep learning methods were used to obtain the best RMSE value (0,4639 m/s² for Inception ResNet v2, with a prediction speed of 11 obs/s).

Conclusions: The proposed method (homomorphic mapping and machine learning) is a valid alternative for calculating acceleration from invariant motion blur in real-time applications when additive noise is not dominant, even surpassing the deep learning techniques evaluated.

Keywords: acceleration, computer vision, deep learning, machine learning, motion blur, vision-based measurement

Article history

Received:
25th/Oct/2022

Modified:
31st/Aug/2023

Accepted:
16th/Nov/2023

Ing., vol. 29, no. 1,
2024. e20057

©The authors;
reproduction right
holder Universidad
Distrital Francisco
José de Caldas.

Open access



*  **Correspondence:** jacoper@utp.edu.co

Resumen

Contexto: Los sistemas de medición basados en visión (VBM) están ganando popularidad como una alternativa asequible y apta para aplicaciones científicas y de ingeniería. Cuando se utilizan cámaras como instrumentos, el desenfoque de movimiento suele surgir como una degradación de imagen recurrente e indeseable, que de hecho contiene información cinemática que normalmente se descarta.

Método: Este artículo introduce un enfoque alternativo para medir la aceleración relativa a partir de una imagen borrosa real de movimiento lineal uniformemente acelerado invariante. Esto se hace utilizando mapeo homomórfico para extraer la *point spread function* (PSF) característica de la imagen borrosa, así como regresión de aprendizaje automático. Se tomaron un total de 125 imágenes borrosas de movimiento uniformemente acelerado en un entorno de luz y distancia controladas, en cinco aceleraciones diferentes en un rango de 0,64 a 2,4 m/s². Este estudio evaluó 19 variantes tales como ensambles de árboles, procesos Gaussianos (GPR) y regresión lineal, regresión con máquina de vectores de soporte (SVM) y regresión con árboles.

Resultados: El mejor resultado de RMSE corresponde a GPR (Matern 5/2), con 0,2547 m/s² y una velocidad de predicción de 530 observaciones por segundo (obs/s). Además, se utilizaron algunos métodos novedosos de aprendizaje profundo para obtener el mejor valor de RMSE (0,4639 m/s² para Inception ResNet v2, con una velocidad de predicción de 11 obs/s).

Conclusiones: El método propuesto (mapeo homomórfico y aprendizaje automático) es una alternativa válida para calcular la aceleración a partir del desenfoque de movimiento invariante en aplicaciones en tiempo real cuando el ruido aditivo no es dominante, incluso superando las técnicas de aprendizaje profundo evaluadas.

Palabras clave: aceleración, visión artificial, aprendizaje profundo, aprendizaje automático, desenfoque de movimiento, medición basada en la visión

Table of contents

	Page		
1. Introduction	3	3. Methodology	14
1.1. Acceleration model for linear motion blur	4	3.1. Rig setup parts	15
1.2. Kinematic quantities using vision-based approaches	6	4. Experimental results	16
1.2.1. Motion blur approaches	7	4.1. Instrument calibration	17
1.2.2. Multi-frame approaches	8	4.2. Data acquisition results – Machine learning	18
1.3. Works related to machine learning	10	4.3. Data acquisition results – Deep learning	19
1.4. Works related to deep learning	10	5. Discussion	20
2. Proposed measurement method	12	6. Conclusions	22
		7. Author Contributions	22
		References	22

1. Introduction

Vision-based measurement (VBM) systems use cameras as an instrument (1). This emerging trend is becoming increasingly popular as an affordable and suitable alternative for many applications such as on-road vehicle detection, tracking, behavior understanding (2), robotics (3), physics (4), biology (5), and engineering (6).

This work introduces a method to calculate acceleration from a real uniformly accelerated motion-blurred image. It uses homomorphic mapping to extract the characteristic point spread function (PSF) of the degraded image, in order to train a machine learning regression model with 125 known instances and responses that finally predicts acceleration as a regression. This approach considers the motion angle to be equal to zero, even though constant acceleration is obtained from an inclined slider. The ground-truth acceleration of each blurred image was measured independently since the sliding camera platform's friction could slightly change the acceleration from measurement to measurement.

Homomorphic filtering is widely used in several applications, as shown in (7, 8), and (9). Although image restoration based on homomorphic filtering is a usual task in image processing, this approach has not been proposed in the literature for acceleration estimation. Homomorphic filtering objectively enhances the image but does not calculate acceleration in the filtering process.

There are two classes of acceleration measurement techniques. The first one involves direct measurements carried out by accelerometers without the need for individual calculations. These accelerometers can be classified based on their operation principle: the piezoelectric effect, the capacitive effect, microelectromechanical systems (MEMS), and the electromechanical servo principle. Some drawbacks of this class are that they are range-fixed, more expensive, and invasive. Direct measurement accelerometers usually need wires that run from the moving target to the analysis system. In some cases, cables can negatively influence the action measured (4). The second class is indirect measurements, where acceleration is estimated from another kinematic variable, using circuits or a computational algorithm.

Kinematic quantities, such as acceleration, are related to the forces that engineering structures can support (10). For instance, some constructions such as floors, footbridges, buildings, and bridges must be continually monitored to evaluate their structural safety (11). Usually, motion sensors need to be connected to a monitoring system, which is often hard to place due to wiring and power issues. Some vision-based displacement measurement systems have been recently developed for structural monitoring because they overcome the already listed issues (6, 12).

Motion, velocity, and acceleration are related to kinematic quantities through time. This means that it is possible to obtain one from another via integration or differentiation. The differential of displacement is called velocity, and the differential of velocity is *acceleration*. Conversely, the integral of acceleration is velocity and, if velocity is integrated, displacement is obtained. In real-world applications, integration is widely used due to its beneficial noise attenuation. Differentiation, on the contrary, amplifies noise.

This makes acceleration more suitable for calculating other kinematic quantities when initial conditions are known. Lastly, it is noteworthy that knowing the instant acceleration provides information about the physical forces applied to moving systems which other quantities cannot supply (13).

Machine learning methods involve mathematical techniques that automatically provide systems with the ability to learn, improve, and predict from training data without being explicitly programmed to do so (14).

Classification and regression are the main tasks of supervised machine learning. The first predicts the specified class to which some input variables belong, and the second one calculates a numerical value within a range that does not necessarily correspond to an exact, previously trained response, as classification indeed does.

The well-known linear regression model assumes a direct relationship between the input variables and the response. Linear regression is the most manageable regression model, as it is effortless to follow and code. Furthermore, it is faster when compared to other approaches. Sensitivity to outliers is one of the drawbacks, which affects its prediction accuracy (15).

In this regard, the Gaussian process regression (GPR) is a Bayesian learning algorithm that has recently gained significant attention due to its usability and accuracy in multivariate regression. GPR considers the joint probability distribution of model outputs to be Gaussian. It shows the predictors as a linear combination of nonlinear basis functions instead of a linear combination of coefficients, as other approaches do (16,17). Our study also used support vector machines (SVMs) because of their efficiency in multi-variable spaces. Furthermore, they are suitable for regression when the data's dimensionality is greater than the number of instances, which was the case (18). Even though the method's main characteristics are known, we assessed one by one with the PSF data obtained from the extraction.

1.1. Acceleration model for linear motion blur

The PSF plays an essential role in image formation theory. All-optical systems have a characteristic PSF, which intrinsically describes the degradation process of the image during its formation. Therefore, the PSF can include information about kinematic quantities such as motion, velocity, and acceleration over the exposure time.

Its nature can classify blur as optical, mechanical, and medium-induced blur (19). This document only considers the mechanical blur that happens when the objects and the camera that captures the image move during the exposure time of the light sensors (20).

A formulation for the PSF in the presence of accelerated motion (introduced in (21)). Even though this research focused on image formation on light-sensitive emulsion film during exposure, it has been a reference for many modern types of research, given its visionary usability in digital image processing.

This PSF model of linear uniformly accelerated motion is shown in Eq. (1):

$$h(x, y) = \begin{cases} \frac{1}{T(v_0^2 + 2ax)^{\frac{1}{2}}} & 0 \leq |x| \leq L \\ 0 & \text{otherwise} \end{cases} \quad (1)$$

where a , v_0 , x , and T are the values of the uniform acceleration, the initial velocity, the displacement, and the exposure time interval, respectively. Fig. 1a illustrates the PSF for constant velocity, and Fig. 1b does so for constant acceleration. Notice that Eq. (1) becomes Eq. (2) when $a = 0$, which corresponds to a uniform velocity. The product Tv_0 is equal to L , the blur's length. Additionally, the Fourier Transform of both is depicted in Figs. 1c and 1d, respectively. Moreover, note that a constant acceleration causes a smear in the Fourier Transform of the PSF, which complicates parameter extraction.

$$h(x, y) = \begin{cases} \frac{1}{Tv_0} & 0 \leq |x| \leq L \\ 0 & \text{otherwise} \end{cases} \quad (2)$$

We cannot infer where the camera is moving towards using the PSF shown in Eq. (1). When the capture system is moving at a constant velocity, the PSF is symmetrical with respect to the y -axis. It does not provide any clue as to whether the motion is from right to left or from left to right. A particular situation arises when the system is accelerated. When this happens, the initial velocity is different from the final one, so the PSF curve is not symmetrical. There are two cases: if the initial velocity is lower than the final one (positive acceleration), the PSF curve is higher on the left side. On the contrary, when the final velocity is lower than the initial one (negative acceleration), the function is higher on the right. Thus, the PSF does not allow determining the motion's direction.

When the camera is not operating horizontally, the angle of motion can be measured regardless of the velocity and the acceleration if the motion blur is long enough.

In some cases, such as velocity estimation, the PSF height $\frac{1}{Tv_0}$ is not explicitly required. Velocity can be calculated using the blur length L and the exposure time T , although height is also related to the initial velocity (Fig. 1a). On the other hand, acceleration can be calculated using Eq. (3). The blur length L in pixels can be obtained from the inverse Fourier transform of Fig. 1d. However, to estimate the acceleration a , information about the change in velocity $v_f^2 - v_0^2$ is also needed. Although v_0 and v_f are, at first glance, inferable from the PSF (Fig. 1b), they do not correspond to the values obtained, since the extracted PSF is also altered by the exposure time, the brightness, the contrast, the noise, and the image's frequency content, among other aspects.

$$a = k \frac{(v_f^2 - v_0^2)}{2L} \quad (3)$$

Some authors have concluded that uniform acceleration causes less degradation to the image than uniform velocity (22–24). Partly for this reason, it is more difficult to estimate acceleration than velocity from a single motion-blurred image. As an example, Fig. 2 depicts the difference between constant velocity and accelerated motion. Most frequency methods use the zero crossings of the collapsed Fourier transform of the motion-blurred image to estimate the blur length (25–28). The zero crossing

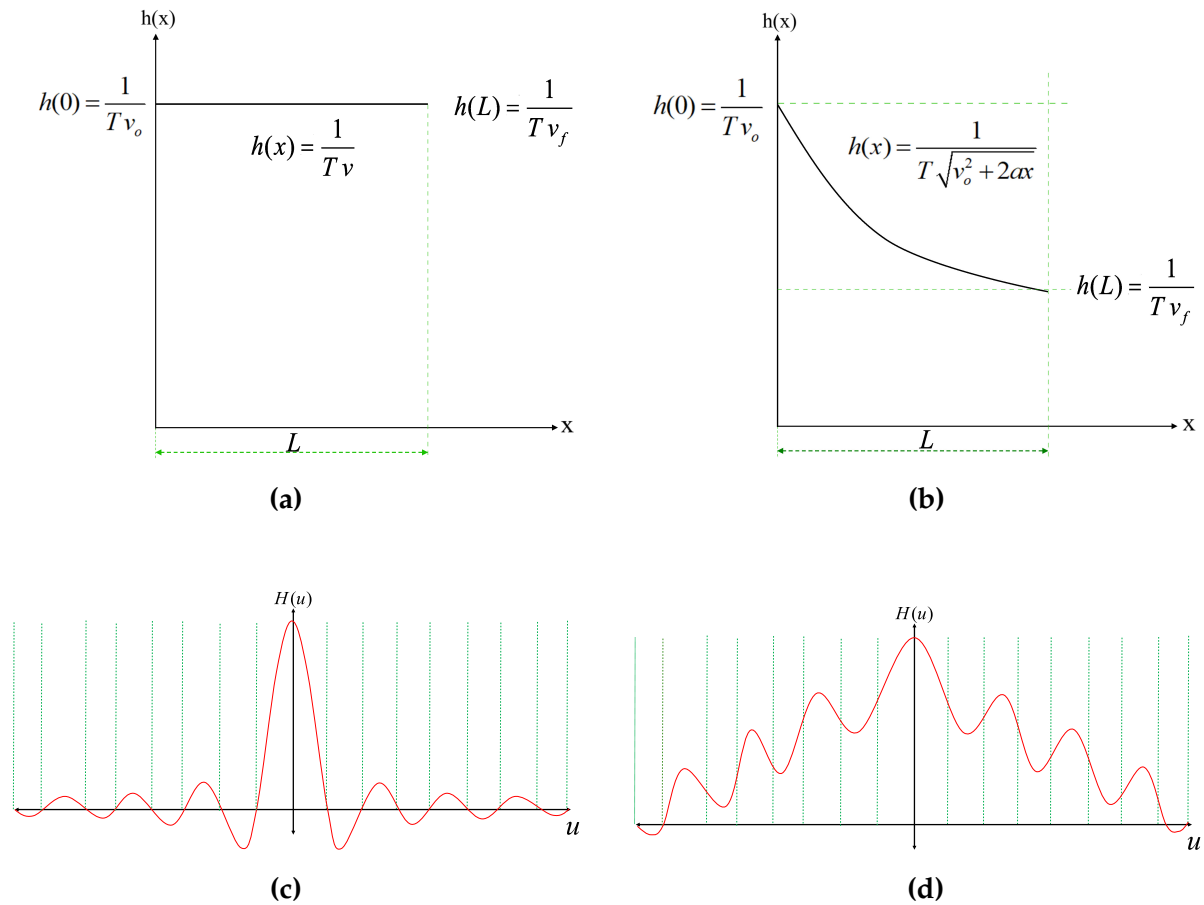


Figure 1. PSF for (a) uniform velocity and (b) uniformly accelerated motion. (c) Fourier transform of the PSF in (a) and (d) Fourier transform of (b). These are only illustrative examples

values are inversely related to the PSF length. When a uniformly accelerated blur degrades the image, its Fourier transform valleys move away from the zero-crossing line axis.

1.2. Kinematic quantities using vision-based approaches

The PSF has an essential role in image formation theory. All-optical systems have a characteristic PSF, which intrinsically describes the degradation process of the image during its formation. Therefore, the PSF can include information about kinematic quantities such as motion, velocity, and acceleration over the exposure time.

Its nature can help to classify blur as optical, mechanical, and medium-induced blur (19). This document only considers the mechanical blur that happens when the objects and the camera capturing the image move during the exposure time of the light sensors (20).

1.2.1. Motion blur approaches

(20) and (29) introduced a way to calculate the speed of vehicles from a single motion-blurred picture, with the aim of supporting transit authorities. Their proposal used the geometry of the scene, the camera parameters, and the blur length. These authors stated that their method's error was less than 10% when applied in real speed detection scenarios.

(30) suggested an approach to measure the speed of a vehicle using motion blur analysis which involves inspecting the speedometer of automotive vehicles. Speed was calculated by analyzing the characteristics and regularities in a single blurred image of a simulated road surface. The authors reported errors of less than 10%. Moreover, there is some research on speed estimation from actual motion-blurred, as is the case of (31,32), and (33).

(34) used code exposure for the accurate reconstruction of motion-blurred images. They proposed statistical blur calculations to obtain precise motion measurements of constant velocity, constant acceleration, and harmonic rotation in actual pictures. For their experiments, they took pictures of a toy car that slid freely on a tilted track only under the influence of gravity. Alternatively, they generated harmonic rotation by using a pendulum-like system. The authors set the camera at the same angle as the tilted platform in order to make the blur almost horizontal in the captured image. They validated their method by measuring the quality of de-blurred images. These authors only estimated motion because their work was mainly focused on image restoration, which does not require a precise reconstruction of the point spread function to improve the image. Their study was based on (35).

(36, 37), and (38) introduced a method for estimating the velocity of a vehicle using a camera moving in the opposite direction to generate blur. They argued that the inclination of the motion blur pattern line in a single image was inherently linked to the velocity of the vehicle and the modulation speed. They also denoted that the inclination level could be calculated by employing line detection techniques such as the Hough transform or the Gabor filter. They estimated that the absolute velocity error was below 2,13 km/h and concluded that their method was independent of the exposure time. Lastly, they inferred that their proposal could be used for vehicular technology.

(39) introduced a defocus correction procedure to obtain the velocity of particles from a single-frame and singleexposure image (SFSEI). They based their proposal on the changes in focus, size, and shape of particles, both close and distant, captured in a blurred snapshot. This method was confirmed in a free-falling particle experiment.

(40) presented a method to determine the position and calculate the velocity of an object by locating the blur's initial and final position. The researchers noticed that, under constant illumination, the motion's start and end could not be determined. To solve this issue, they used modulated illumination, i.e., red light at the beginning and blue light at the end, in order to tag the blurred image. They reported that their method had not yet been implemented in real conditions.

The work by (42) and (43) introduced a technique to calculate velocity from a single linear motion-blurred picture. The discrete cosine transform was used to extract the PSF of the actual motion-blurred images as a basis to measure the blue extent L and the angle. This was done in combination with the exposure time T .

(44) proposed a novel approach involving adversarial blur attack against visual object tracking algorithms. Rather than adding imperceptible noise, they actively synthesized natural motion blur on video frames in order to mislead state-of-the-art trackers. The attack was performed by tuning two sets of parameters controlling the motion pattern and light accumulation process that generate realistic motion blur. An optimization-based attack iteratively solved an adversarial objective function to find the blurring parameters. A one-step attack predicted the parameters using a trained neural network. Experiments on four tracking benchmarks demonstrated significant performance drops for multiple trackers, showing the threat of adversarial motion blur. The key contributions of this work were introducing adversarial motion blur as a new attack angle and designing optimization and learning-based approaches to craft natural adversarial examples. The limitations included heavy computation loads for the optimization attack and reliance on a specific tracker for training examples. All methods proposed by the authors used video frame sequences instead of a single image, and this attack revealed the brittleness of trackers against common video corruptions, thus motivating the development of robust motion-blur algorithms.

1.2.2. Multi-frame approaches

(45) introduced a cell segmentation and competitive survival model (CSS) together with the traditional methods of particle image velocimetry (PIV). They used their algorithm with actual and artificial pictures and made comparisons with other strategies.

(3) presented a system to estimate the position, velocity, and acceleration of a planar moving robot using a calibrated digital black-and-white camera and light emission diodes as markers. They employed a multi-frame approach that made use of the Kalman filter to calculate velocity and acceleration. These authors stated that the blur motion should be limited, so that the exposure time was short when compared to the change in the position of the light markers. They concluded that their video approach method is accurate, but they suggested that using a faster CCD sensor would yield better results.

(4) suggested an acceleration measurement approach using various synchronized video cameras based on videogrammetric reconstructions. Their method located the centroid of visible marks set by the researchers on a shaft run by a shaker. They built a prototype to carry out the proof of concept. They also attached some calibrated accelerometers directly below the target marks in order to obtain ground-truth data to compare with their results. They calculated the second derivative of the videogrammetric position data using the seven-point numerical algorithm to estimate the acceleration. Finally, they provided some overlapped plots aimed at contrasting their results to the accelerometer's measurements. They concluded that their results were similar to those obtained using accelerometers. No error was explicitly calculated.

(13) proposed a variational method to estimate the acceleration of dynamic systems based on image sequences. They stated that their approach went further than the traditional optical flow methods because they can calculate acceleration. They also pointed out that fluid flow images for calculating acceleration have not been thoroughly studied, even though they are of significant interest. They suggested the use of acceleration fields and an energy function for their calculations, relying on space-time constraints. When they confronted their results to ground-truth data, they estimated a 7% average relative error.

Moreover, (46) described a non-invasive method to estimate the pressure distribution in a flow field while employing PIV.

(47) proposed an approach to measure the speed of a rotating item. They used a pair of cameras to capture a temporal sequence of pictures from coded targets (CTs), which were set on the rotating surface of the object to work as visual marks. This feature matching-based algorithm depends on the motion estimation of contiguous target image pairs. In their experiments, the authors used a rotating fan at 120 rpm and a convolutional neural network (CNN) to identify changes in the position of the CTs during the exposure time. Even though they did not explicitly calculate the speed of the blades, they concluded that their method benefits high-speed object measurement applications. This technique used multiple consecutive images to calculate speed and acceleration.

(48) introduced a computationally efficient computer vision method to estimate the trunk's flexion angle, angular speed, and angular acceleration during lifting by extracting simple bounding box features from video frames. Regression models estimated trunk kinematics from these features. The advantages of this approach are computational efficiency, non-intrusiveness, and the potential for practical lifting assessments in the workplace, and its limitations include reliance on simulated training data and lower precision than motion capture methods. This study demonstrated the feasibility of using simple video features to estimate biomechanical quantities related to injury risk, allowing for automated ergonomic evaluation over extended periods.

In their review, (49) covered deep learning methods for the estimation of fluid velocity fields, including fluid motion estimation from particle images and velocity field super-resolution reconstruction. Supervised and unsupervised convolutional neural network approaches have shown excellent performance in estimating fluid motion from particle image pairs. GAN and physics-informed neural network methods have also shown potential for the high-resolution reconstruction of velocity fields. The key advantage of deep learning is the ability to learn feature representations directly from data, thus surpassing traditional methods. Limitations included the need for extensive training datasets and difficulties in incorporating physical knowledge. All reviewed methods used video sequences or image pairs for estimation. Overall, this review demonstrated that computer vision and deep learning hold great potential for estimating kinematic quantities in fluid flow and human biomechanics applications, with anticipated growth in the future integration of these methods.

Further reading about PIV acceleration measurement can be found in (50) and (51), and other multi-frame video strategies for velocity are shown in (52,53), and (54).

1.3. Works related to machine learning

(55) used support vector machines (SVM) regression to forecast water flow velocity. Even though they asserted that their approach was not fully successful – as expected –, it was promising and useful for future research.

(56) suggested a method for estimating the velocity profile of small streams by using robust machine learning algorithms such as artificial neural networks (ANNs), SVMs, and k-nearest neighbor algorithms (k-NN), with the latter outperforming the others in the results.

(57) introduced a machine learning approach based on a CNN model to estimate velocity fields using PIV with missing regions. These authors also argued that, despite recent advances, no studies have focused on machine learning applications using this approach. They used artificial images generated with a direct numerical simulation, concluding that it is possible to estimate the velocity fields with less than 10 % error.

The work by (58) should be highlighted, as they suggested a method to assess structural damage by estimating acceleration at multiple points via a traditional sensor approach. Alternatively, they interpreted the results using the supervised machine learning algorithm called *random forest*.

As mentioned above, some remarkable studies have been carried out to estimate velocity and acceleration from multi-frame and multi-camera methods. However, we did not find any strategy based on motion-blurred images for measuring acceleration.

1.4. Works related to deep learning

Deep learning is a technique derived from neural networks that has recently supported instrumentation and measurement. In the scientific literature, it can already be found in combination with traditional instrumentation, such as light detection and ranging (LiDAR) (59), radars (60), and PIV (61, 62), in order to estimate the velocity of objects and particles. However, we found no evidence of similar works using deep learning and a single motion-blurred image.

Estimating kinematic quantities from a single image is a challenging yet potentially beneficial issue. A moving system, such as a vehicle, a robot, or a drone, can use motion-blurred images to estimate these parameters without the need for bulkier, heavier, and more expensive devices. Moreover, processing one image is often easier than processing a video sequence.

The contributions of this study are as follows:

- The construction and metrological calibration of an electromechanical incline slider to generate different acceleration values.

- The development of a dataset with 125 invariant, uniformly accelerated motion-blurred images in a controlled environment.
- The comparison of some machine learning techniques against deep learning for acceleration estimation.

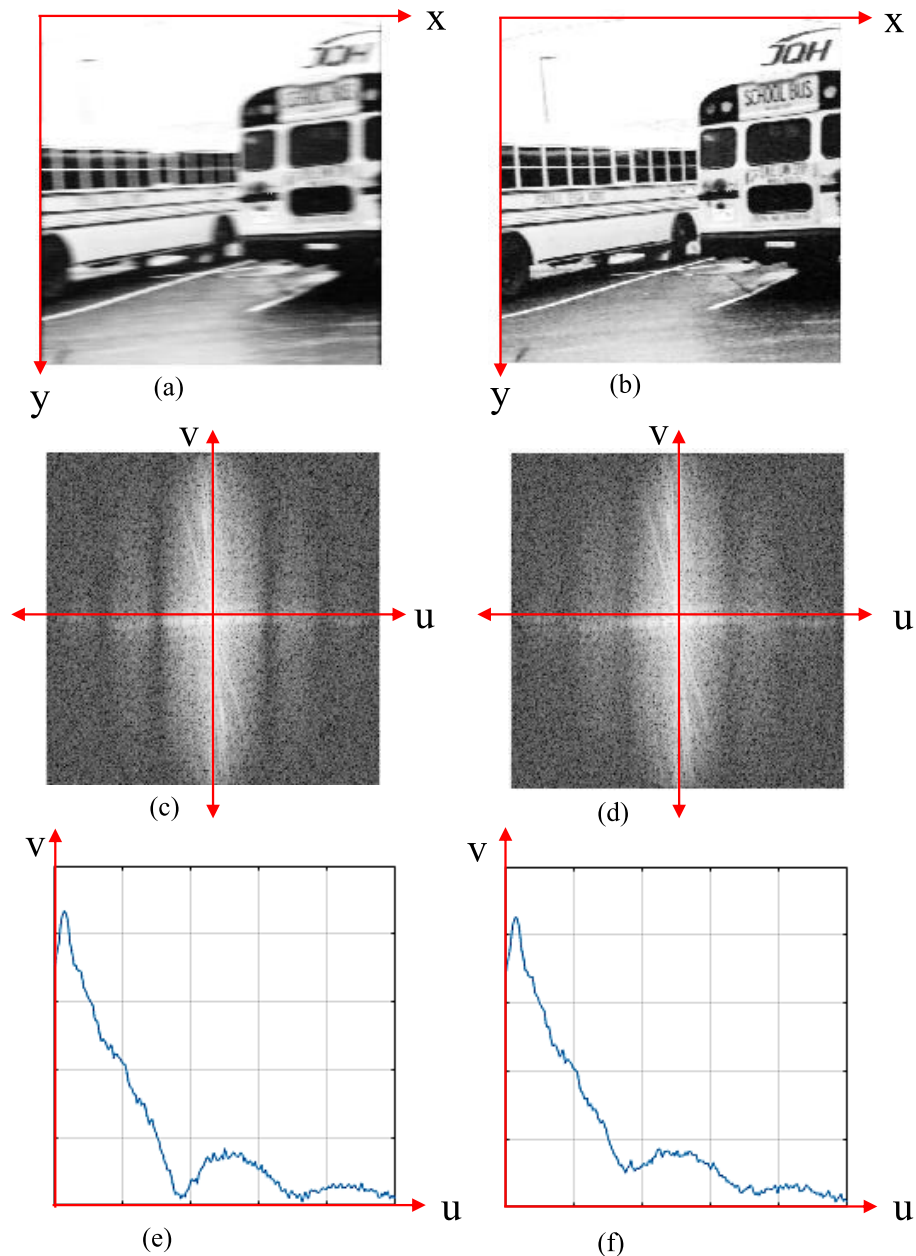


Figure 2. Differences between a degraded image with a uniform and a uniformly accelerated motion blur. (a) Invariant motion-blurred image related to constant velocity. Here, the blur is more visible to the naked eye. (b) Invariant motion-blurred image related to constant acceleration. Here, the blur is lower. (c) Modulation transfer function of (a). (d) Modulation transfer function of (b). (e) Collapsed MTF on the u -axis of (c). (f) Collapsed MTF on the u -axis of (d)

- A proposal for the estimation of acceleration from a real single invariant, uniformly accelerated motion-blurred image.

The remainder of this paper is organized as follows. Section 2 introduces our proposal for acceleration estimation using machine learning and the PSF as a source of characteristic feature patterns. Section 3 presents the experimental setup and the testing carried out. Section 4 outlines the results obtained in the experiments by comparing different regression approaches (including deep learning) and their metrics. Section 4 contrasts the results with those of previous authors and discusses the limitations and benefits of the method. Finally, Section 5 presents the conclusions of this work.

This paper is a product of and reuses, with due authorization, content from the PhD thesis and research project entitled “A contribution to the estimation of kinematic quantities from linear motion-blurred images” cited in (43).

2. Proposed measurement method

An image system is modeled as the convolution of the PSF with the blur-free image. This does not allow for the use of linear filtering approaches to extract the PSF. Alternatively, homomorphic filtering uses nonlinearity transformations, such as logarithmic transformations, to map convolution into a separable linear additive domain (63–66). As a theoretical basis, this research used the homomorphic filtering principle to extract the PSF.

Consider that $g(x, y)$ corresponds to the degraded blur image, $i(x, y)$ is the blur-free image, and $h(x, y)$ represents the degradation kernel (PSF). If noise of any kind is not added and the blur system, it is considered to be linear and stationary, and the process can be described as seen in Eq. (4):

$$g(x, y) = i(x, y) * h(x, y) \quad (4)$$

The product $*$ denotes convolution in two dimensions. Additionally, the image convolution from (4) can be also represented as an integral, as shown in Eq. (5):

$$i(x, y) * h(x, y) = \int_{-\infty}^{+\infty} \int_{-\infty}^{+\infty} i(x', y') h(x - x', y - y') dx' dy' \quad (5)$$

Considering that Eq (5) deals with finite blur images in space, it is defined in the intervals $x_2 \leq x' \leq x_1$ and $y_2 \leq y' \leq y_1$. It should be noted that the convolution interval must be larger than the PSF interval of the blur.

Now, the discrete Fourier transform (DFT) is applied to both sides of Eq. (4) to obtain Eq. (6), which represents a point-wise multiplication in frequency domain instead of a convolution in space.

$$G(u, v) = I(u, v)H(u, v) \quad (6)$$

$G(u, v)$, as shown in (6), is a complex value, so it can also be written in polar coordinates using magnitude and angle, as shown in Eq. (7).

$$|G(u, v)|e^{j\phi_G} = |I(u, v)|e^{j\phi_I}|H(u, v)|e^{j\phi_H} \quad (7)$$

This relation can be split into magnitude and phase components, as shown in Eqs. (8) (10), respectively.

$$|G(u, v)| = |I(u, v)||H(u, v)| \quad (8)$$

$$\begin{aligned} \phi_G &= \text{ang}[I(u, v) + H(u, v)] \\ \log |G(u, v)| &= \log |I(u, v)H(u, v)| \end{aligned} \quad (9)$$

Only the log magnitude portion of the complex logarithm of the DFT is used, as shown in Eq. (10).

$$\log |G(u, v)| = \log |I(u, v)| + \log |H(u, v)| \quad (10)$$

Although some images can be very different in space, their average frequency is usually very much alike and almost indistinguishable to the naked eye. This allows using the average of Q hypothetical blur-free images $I(u, v)_k$ to estimate the prototype clear blur-free image $P(u, v)$ in frequency, as shown in Eq. (11) (65).

$$P(u, v) = \frac{1}{Q} \sum_{k=1}^Q I(u, v)_k \quad (11)$$

in such a way that

$$\log |I(u, v)| \cong \log |P(u, v)| \quad (12)$$

$$\log [I(u, v)] \cong \frac{1}{Q} \sum_{k=1}^Q \log |I(u, v)_k| \quad (13)$$

Replacing Eq. (13) into Eq. (10), and then solving for $|H(u, v)|$,

$$|H(u, v)| \cong \exp \left[\log |G(u, v)| - \frac{1}{Q} \sum_{k=1}^Q \log |I(u, v)_k| \right] \quad (14)$$

where $|H(u, v)|$ is the modulation transfer function (MTF) of an arbitrary blur, which can be estimated without knowledge of the actual blur-free image using a set of Q reference images to generate a prototype-average log spectrum.

Even though the classical approach for the PSF estimation of an image suggests using statistically close images to generate the prototype average log spectrum, this study used 5 still background images as the clear image in order to estimate the MTF only once for all the experiments. $Q = 5$ was recommended in (65). Subsequently, the inverse Fourier transform (*iDFT*) of $H(u, v)$ is applied to obtain $h(x, y)$, the PSF, as seen in Eq. (15).

$$h(x, y) = iDFT(H(u, v)) \quad (15)$$

Fig. 3 presents the proposed method for acceleration estimation using homomorphic filtering and machine learning regression. In this method, five blur-free images $i(x, y)_k$ are taken to the unchangeable background with the camera at rest. This helps reduce the additive noise, subtracting the average of a set of hypothetical blur-free images. Consequently, the MTF is obtained for each of the five images and then averaged, added, and divided by five. This yields a prototype blur-free background $\log |P|$,

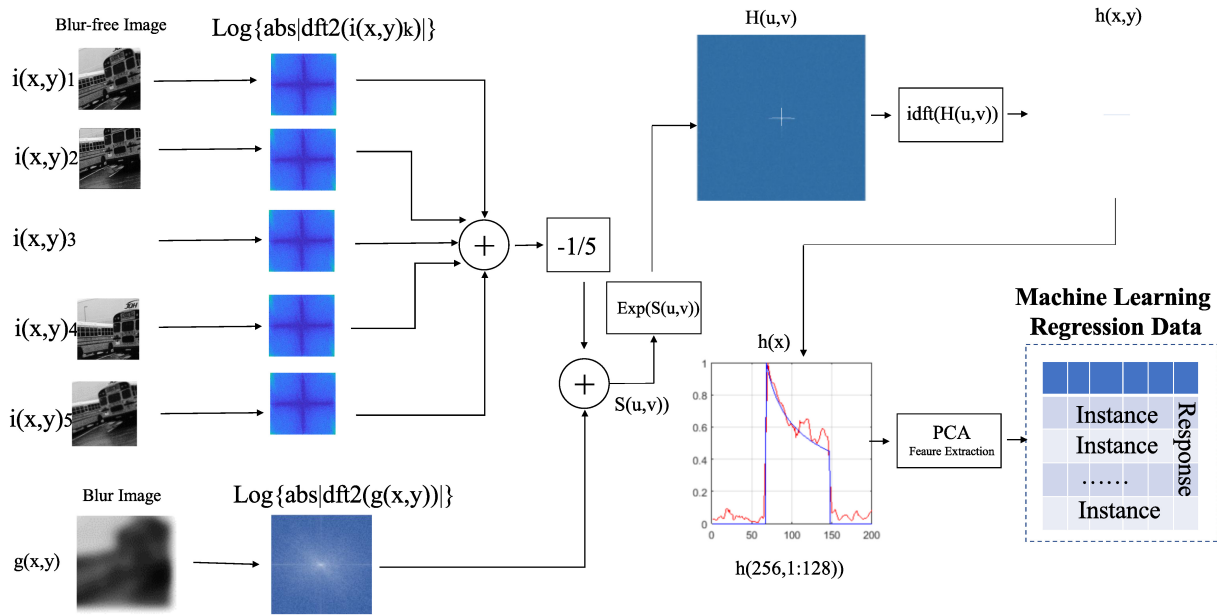


Figure 3. Diagram depicting the process followed to estimate acceleration using homomorphic filtering while applying machine learning. Some blur-free images of the background are needed to separate the PSF for training

which is subtracted from the MTF of the motion-blurred image $\log |G(u, v)|$ to obtain the output $s(u, v)$. Afterwards, the exponential function is used to remove the logarithm. This allows obtaining the optical Fourier transform $H(u, v)$ of the blurred image, which leads to the PSF $h(x, y)$ in two dimensions via the inverse Fourier transform. As the motion occurs only in the horizontal axis, the actual PSF in one dimension $h(x)$ can be extracted from the central horizontal line of the PSF $h(x, y)$.

Therefore, this research took only the central horizontal row of the inverse Fourier transform, yielding a one-dimension vector containing the characteristic PSF.

If the motion is not horizontal, the one-dimension PSF can also be extracted, but the angle of rotation of the line must be estimated and then rotated. This angle can be calculated using the Radon transform, the Hough transform (42), or principal components analysis (PCA).

Before training, the instances are space-reduced to avoid redundancy using PCA. Finally, a set of uniformly accelerated motion-blurred images with a known acceleration is used for training.

3. Methodology

The experiments presented in this section were carried out to measure constant acceleration from a linear motion-blurred image by using homomorphic filtering to extract the PSF and machine learning to predict the actual response. First, all parts of the rig setup are introduced, with the purpose of providing a more detailed description of the procedure. Then, an overview of the aforementioned machine learning

and deep learning methods is presented, and, finally, the evaluation metrics are described regarding the regression methods evaluated.

3.1. Rig setup parts

This section shows the materials and the laboratory equipment needed for the experiments, some of which were specifically constructed within the framework of this study.

Slider

A 185-cm-long aluminum slider constructed for previous speed experiments was used (42), which was slightly modified for our study. Fig. 5 shows the physical layout parts modeled in order to validate the proposed method. Five preset posters were used as a background scene (Fig. 4). Additionally, the camera was placed in parallel to and 171 cm away from the rig. An inclinometer was also installed on the camera. A constant acceleration was achieved by raising an end of the platform to one of the five possible preset angles (A1, A2, A4, A5, and A7) listed in Table I. Sliding occurred evenly and only under the force of gravity. Fig. 6 presents the rig setup used to carry out the experiments. More information about its construction and calibration can be found in (67).

Image analysis system

Motion-blurred image capture and processing were performed on a 64-bit desktop computer with a Core I3 processor and 2GB RAM. Additionally, a 64-bit laptop computer with an AMD A3 processor and 2GB RAM was used for analyzing the acceleration data from the controller system. Both computers used Windows 7 and were running MATLAB 2017b.

Images

Our experiments were carried out in a controlled environment. A scientific digital camera (Basler acA2000-165um USB 3.0) (68) was used to take the pictures. In addition, the artificial white light from the led panel lamps was about 255 Lux, the distance to pattern poster was set at 171 cm, the maximum exposure time of the camera was 100 ms, the slider acceleration was between 0,6 and 2,40 m/s², and the aperture of the lens diaphragm (69) was F/4.

Blurred images of five different pattern posters were taken (Fig. 4). Afterwards, the captured digital images were clipped and converted to grayscale (70). These experiments considered the angle of motion at zero degrees. Although the camera slid on an inclined plane, the motion blur was horizontal with respect to the camera angle. The background scene posters were not rotated, so, at the naked eye, they looked crooked. Fig. 5 shows each of the elements described.

PCA feature extraction

Feature extraction is a relevant topic in signal processing, mostly due to the high dimensionality of data and their redundancy (71). PCA is a classical and widely accepted statistical approach for feature

extraction in pattern recognition and computer vision (72). In this study, PCA feature extraction was used to reduce redundant data from the extracted PSF. The multidimensional space was transformed from 125 to 76 characteristics.

Machine learning regression

Five different approaches were used to predict the acceleration from the PSF data of actual motion-blurred images. Tree ensembles, Gaussian processes (GPR), and linear, SVM, and tree regression and their variations were evaluated, as presented in Table II.

Regression model assessment

The metrics applied to assess the regressions were the root mean square error (RMSE), the prediction speed in observations per second, and the training time in seconds.

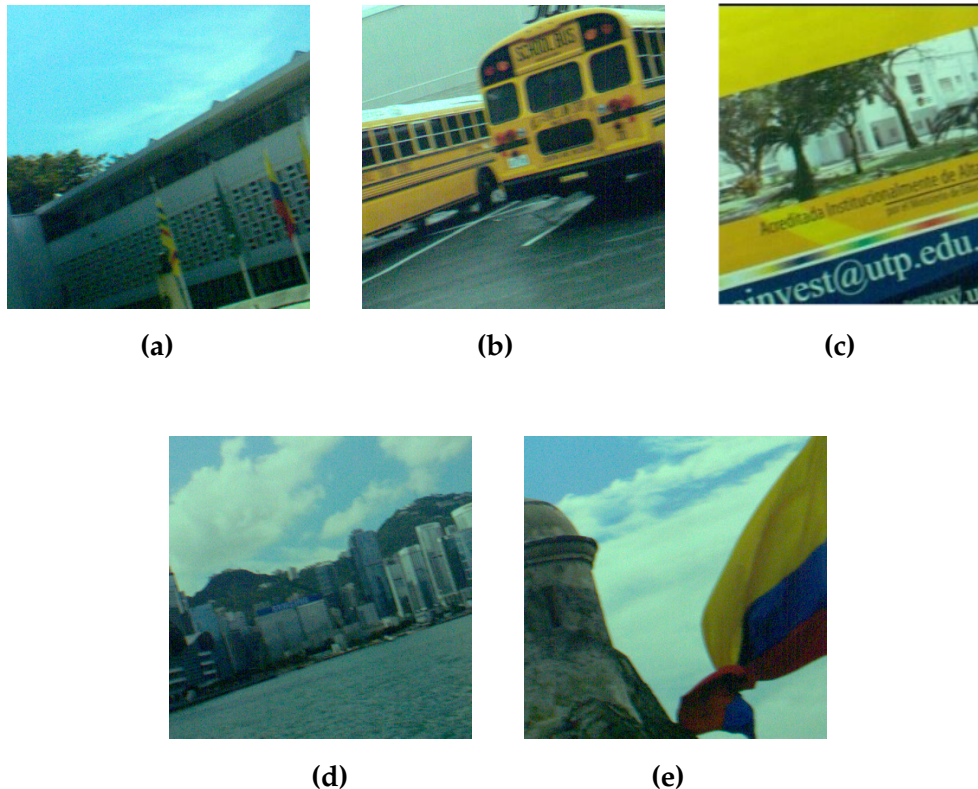


Figure 4. Color version of some accelerated motion-blurred images. The degradation is almost imperceptible by visual inspection

4. Experimental results

Five pictures were taken at each of the five preset accelerations. Additionally, five background scene posters were used, for a total of 125 motion-blurred images.

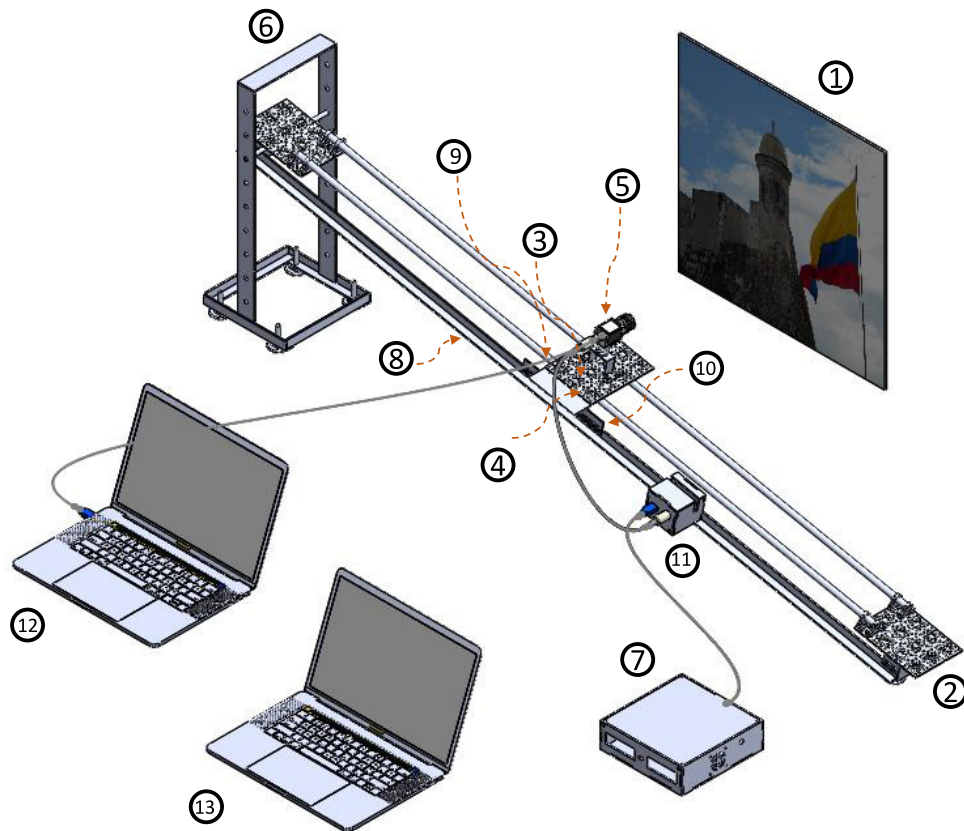


Figure 5. Setup parts and their location. Background pattern poster (1), leveling rubber feet (2), digital pitch gauge-inclinometer (3), camera sliding carriage platform (4), camera (5), lifting base (6), controller (7), oiled stainless steel rods (8), low-friction linear bearings (9), laser-cut toothed steel sheet (10), camera trigger (11), image capture computer (12), and data analysis computer (13)

Although the acceleration values were almost always the same as in Table I, the error was estimated individually using the electromechanical instrument and our vision-based acceleration values.

4.1. Instrument calibration

The uniformly accelerated motion system involved an Arduino Nano microcontroller, which was responsible for measuring the time it took to block each tooth of the steel sheet. Its operation consisted of allowing the camera carriage platform on the steel rods to slide at five different angles, yielding different accelerations depending on the height. The angles and their accelerations are shown in Table I.

Calibration was performed by measuring the acceleration with both the controller system and the Phywe Cobra4 Sensor-Unit 3D-Acceleration standard instrument (± 2 g and a resolution of 0,001 g), using the Cobra4 wireless link to transmit the acceleration data (73). The combined uncertainty and the sensitivity coefficients were evaluated to estimate the total expanded uncertainty according to guidelines regarding the expression of uncertainty in measurement (74,75). See (67) for more detailed information about the calibration process.



Figure 6. Rig setup to generate uniformly accelerated motion-blurred images

Table I. Acceleration values and uncertainties obtained from the calibration procedure

Index	Angle (Degree)	Acceleration (m/s ²)
A0	15°	2,4630 ± 0,0285
A1	13,3°	2,1782 ± 0,0233
A2	10,1°	1,5416 ± 0,0161
A3	7,9°	1,2292 ± 0,0130
A4	4,5°	0,6448 ± 0,0074

4.2. Data acquisition results – Machine learning

Five folds were used to validate all of the proposed regression models. Table II shows the results for the basic regression models and their variants. Note that, even though only five major approaches were assessed, each one had a subset of variants, for a total of 19. The best RMSE results were reported by GPR (Matern 5/2), linear regression, and SVM (quadratic) regression, with 0,2547, 0,2553, and 0,2843 m/s², respectively. GPR (Matern 5/2), linear regression, and SVM (quadratic) regression reported values of 530, 470, and 540 obs/s, respectively. Finally, the fastest training time corresponded to GPR (Matern 5/2), with 1,373 s. See Table II for more details.

Moreover, predicted *vs.* actual and residuals plots were employed for the best three RMSE results. The residuals plots for GPR (Matern 5/2), linear regression, and SVM (quadratic) regression (Figs. 8a, 8b, and 8c, respectively) showed that the acceleration residuals tend to change their sign from negative to positive when the acceleration is higher than 1,4 m/s². Furthermore, the acceleration residuals are smaller in all cases when the acceleration is higher than 1,0 m/s². This makes GPR (Matern 5/2) more

suitable for real-time applications. In summary, the plots for GPR (Fig. 8a) and linear regression (Fig. 7) are almost identical.

As expected, decision trees showed the worst results since they tend to fail when training data is limited.

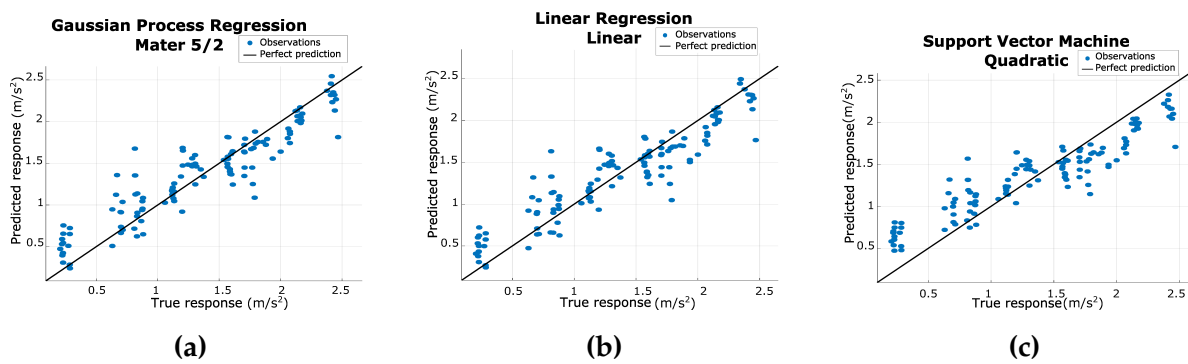


Figure 7. Predicted vs. actual plots for (a) Matern 5/2 regression, (b) Linear regression, and (c) SVM regression

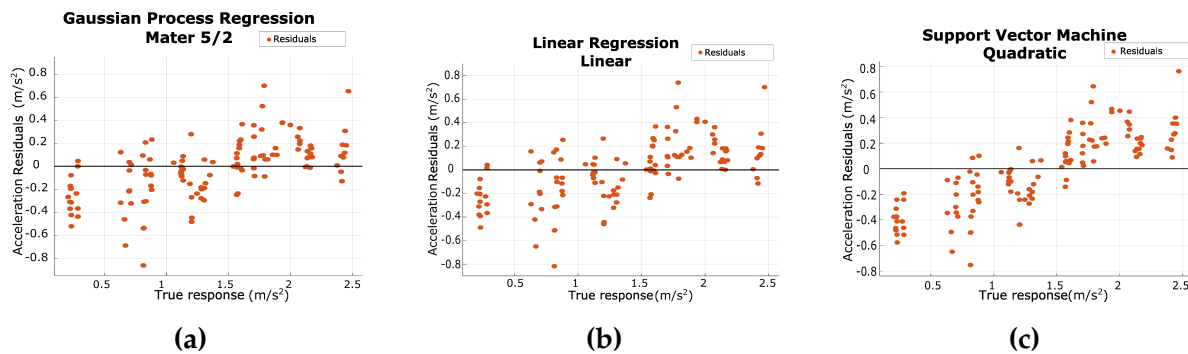


Figure 8. Residual plots for (a) Matern 5/2 regression, (b) linear regression, and (c) SVM regression

4.3. Data acquisition results – Deep learning

Deep learning techniques have some advantages, such as the automatic extraction of features. In addition, input images can be used without any prior processing beyond the geometric transformations of the training images when expanding the dataset becomes necessary. Therefore, in this part of the experimentation process, homomorphic mapping was not used as a source of features for the regression.

The executed algorithms were coded in MATLAB R2020b, using the Deep Network Designer toolbox. It is crucial to emphasize that the learning algorithm corresponds to a regression instead of a classification process, which allows generating response values outside the training data.

As mentioned earlier, 125 training images were used, which were 512 x 512 x 3 pixels in size. However, the pre-trained networks required different dimensions. Therefore, the pixel size of the images was set at 224 x 224 x 3 for GoogleNet and VGG-16, at 227 x 270 x 3 for AlexNet, and at 299 x 299 x 3 for Inception ResNet-v2.

The performance of a CNN depends mainly on hyperparameters such as the learning rate, the mini-batch size, the number of epochs, the number of iterations, and the solver algorithm. For a good performance, a determining factor is the pre-trained model, which typically uses hundreds or thousands of images. Therefore, in our study, it was necessary to extend the image dataset by performing rotations and reflections to obtain 750 images. The image size scale was not changed, as it implicitly includes the blur length attributes.

The dataset was divided as follows: 80 % for training, 10 % for validation, and 10 % for testing. Thus, the 750 images were divided into 600 training images, 75 validation images, and 75 testing images. All of them were randomly selected from the dataset.

As can be seen in Table III, AlexNet offered the shortest training and prediction times while using the GTX1650 and the GTX1050 GPUs. Regarding the RMSE, the lowest value (0,4639 m/s²) was obtained using Inception ResNet v2. However, this is far from what was achieved using homomorphic mapping, which showed a smaller RMSE (0,2547 m/s²).

It should be noted that only GPUs were used with the deep learning algorithms and CPUs with the machine learning algorithms.

5. Discussion

Even though there are some studies on estimating speed using vision-based measurement (VBM), to the best of our knowledge, only a few deal with acceleration. Likewise, there is no evidence of studies that estimate acceleration from a motion-blurred image.

Some approaches have been introduced to measure acceleration, and all of them require at least two consecutive frames (45, 46, 76), while others also use high-speed or multiple cameras (4, 77), thus making make classical approaches more expensive and bulkier.

This field of research has great potential across various applications, including forensic sciences, particle physics, and autonomous drones. The proposed technique can extract essential motion parameters from a single image, simplifying processes that traditionally rely on multiple video frames or complex sensor configurations. Consequently, it reduces the complexities associated with runtime and computation, resulting in substantial savings regarding storage space and energy consumption. This efficiency makes it an environmentally sustainable and cost-effective approach, underscoring its importance.

The acquisition of blurred images relies on the adjustment of camera settings, particularly the exposure time relative to the scene's motion. While creating motion blur is relatively straightforward in general photography, achieving controlled motion blur in scientific or forensic contexts often requires specific conditions. Moreover, analyzing the variables, conditions, or parameters involved in obtaining motion blur becomes more intricate when the subject or object in motion is not the camera itself. In such scenarios, both the camera and the subject's movements affect the resulting blur, necessitating the application of specialized methodologies. The attributes of a camera employed to capture motion blur data are not rigidly prescribed, but several critical features contribute to its effectiveness. These encompass adjustable exposure settings, sensor sensitivity, image stabilization capabilities, and the camera's lens and sensor quality. These attributes significantly influence the quality and reliability of the analysis. Consequently, the selected camera and its settings emerge as a pivotal consideration, with a substantial influence over the outcomes of motion blur analysis in diverse applications.

Table II. Machine learning results obtained using tree ensembles, GPR, and linear, SVM, and tree regression

Regression models	Variant	RMSE (m/s ²)	Prediction Speed (Obs/s)	Training Time (s)
Ensembles of trees	Bagged trees	0,4124	420	1,7598
	Boosted trees	0,3507	480	1,8514
GPR	Exponential	0,3187	460	1,4044
	Matern 5/2	0,2547	530	1,373
	Rational	0,2553	530	1,6424
	Quadratic squared exponential	0,2553	470	1,5473
SVM	Linear	0,2553	470	1,5175
	Coarse	0,6607	510	1,0678
	Gaussian fine	0,4611	480	1,0486
	Gaussian medium	0,5243	500	1,0921
	Gaussian linear	0,3747	500	1,0779
	Quadratic	0,2843	540	1,804
Trees	Coarse tree	0,6327	570	0,9837
	Fine tree	0,4915	540	1,0379
	Medium tree	0,4604	540	1,0037

This alternative blur-based method has benefits. Motion blur is a usual and undesirable degradation, but it is possible to take advantage of it, as it allows for acceleration estimations. In addition, this approach can be implemented with low-cost cameras, instead of high-speed multi-frame video equipment, which is more expensive.

Likewise, the proposed method has some limitations. One is that it needs a set of blur-free images as reference for training. However, in some cases, this is easy to obtain from the background. For example, a drone can obtain the prototype images from an initial image (a prototype with no motion blur) of a crop and then fly over it while estimating the acceleration. Noise is another limitation of this proposal: when the noise is dominant, the extraction of the PSF can fail along with the estimation. Finally, the

Table III. Deep learning results for AlexNet, GoogleNet, VGG-16, and inception ResNet v2

Regression models	Variant	RMSE (m/s ²)	Prediction speed (Obs/s)	Training time (s)
AlexNet	GTX 1050	0,8088	74	125
	GTX 1650	0,6585	52	95
GooleNet	GTX 1050	0,5918	44	667
	GTX 1650	0,6112	43	432
VGG-16	GTX 1050	0,7334	4	1.655
	GTX 1650	0,6377	21	755
Inception ResNet v2	GTX 1050	3,0234	13	8.229
	GTX 1650	0,4639	11	5.582

space-invariant model introduced in this study assumes that the exposure time is relatively short, and the length from the rig setup to the camera is fixed to ensure invariant blur on all images.

6. Conclusions

With some degree of accuracy, the machine learning models successfully estimate relative acceleration from a single motion-blurred image, using homomorphic filtering to extract the features of the PSF, which depends on the initial velocity, the acceleration, and the exposure time, as shown in Eq. (1).

The proposed method is a valid alternative to estimate acceleration with invariant motion blur. The best machine learning methods were GPR (Matern 5/2) and linear regression, with RMSE values of 0,2547 and 0,2553 m/s², respectively. These methods were able to perform 530 and 470 obs/s, respectively. Finally, the best results were obtained when the acceleration was above 1,0 m/s². This makes machine learning an alternative approach that can be used in real-time applications for estimating acceleration when motion blur is invariant, and noise is not dominant.

7. Author Contributions

All authors contributed equally to the research.

References

- [1] S. Shirmohammadi and A. Ferrero, "Camera as the instrument: the rising trend of vision based measurement," *IEEE Instrumentation Measurement Magazine*, vol. 17, no. 3, pp. 41–47, 2014. <https://doi.org/10.1109/MIM.2014.6825388> ↑3
- [2] S. S. Beauchemin, M. A. Bauer, T. Kowsari, and J. Cho, "Portable and scalable vision-based vehicular instrumentation for the analysis of driver intentionality," *IEEE Transactions on Instrumentation and*

- Measurement*, vol. 61, no. 2, pp. 391–401, 2012. <https://doi.org/10.1109/TIM.2011.2164854> ↑3
- [3] P. Dutkiewicz, M. Kielczewski, K. Kozłowski, and D. Pazderski, “Vision localization system for mobile robot with velocities and acceleration estimator,” *Bulletin of the Polish Academy of Sciences: Technical Sciences*, vol. 58, no. 1, pp. 29–41, 2010. <https://doi.org/10.2478/v10175-010-0003-9> ↑3, 8
- [4] J. Leifer, B. Weems, S. C. Kienle, and A. M. Sims, “Three-dimensional acceleration measurement using videogrammetry tracking data,” *Experimental Mechanics*, vol. 51, no. 2, pp. 199–217, 2011. <https://doi.org/10.1007/s11340-010-9352-4> ↑3, 8, 20
- [5] F. Karimirad, S. Chauhan, and B. Shirinzadeh, “Vision-based force measurement using neural networks for biological cell microinjection,” *Journal of Biomechanics*, vol. 47, no. 5, pp. 1157–1163, 2014. <https://doi.org/10.1016/j.jbiomech.2013.12.007> ↑3
- [6] Y. Fukuda, M. Q. Feng, and M. Shinozuka, “Cost-effective vision-based system for monitoring dynamic response of civil engineering structures,” *Structural Control and Health Monitoring*, vol. 17, no. 8, pp. 918–936, 2010. <https://doi.org/10.1002/stc.360> ↑3
- [7] S. Benameur, M. Mignotte, and F. Lavoie, “An homomorphic filtering and expectation maximization approach for the point spread function estimation in ultrasound imaging,” in *Image Processing: Algorithms and Systems X; and Parallel Processing for Imaging Applications II*, International Society for Optics and Photonics, vol. 8295, 2012, 82950T. <https://doi.org/10.1117/12.903785> ↑3
- [8] O. Mattausch and O. Goksel, “Image-based psf estimation for ultrasound training simulation,” in *International Workshop on Simulation and Synthesis in Medical Imaging*, Springer, 2016, pp. 23–33. https://doi.org/10.1007/978-3-319-46630-9_3 ↑3
- [9] A. P. Janwale and S. S. Lomte, “Enhancement of cotton leaves images using various filtering techniques,” in *Data Management, Analytics and Innovation (ICDMAI), 2017 International Conference on*, IEEE, 2017, pp. 303–305. <https://doi.org/10.1109/ICDMAI.2017.8073530> ↑3
- [10] J. Kim, K. Kim, and H. Sohn, “Autonomous dynamic displacement estimation from data fusion of acceleration and intermittent displacement measurements,” *Mechanical Systems and Signal Processing*, vol. 42, no. 1-2, pp. 194–205, 2014. <https://doi.org/10.1016/j.ymsp.2013.09.014> ↑3
- [11] F. Zheng, L. Shao, V. Racic, and J. Brownjohn, “Measuring human-induced vibrations of civil engineering structures via vision-based motion tracking,” *Measurement*, vol. 83, pp. 44–56, 2016. <https://doi.org/10.1016/j.measurement.2016.01.015> ↑3
- [12] D. Ribeiro, R. Calçada, J. Ferreira, and T. Martins, “Non-contact measurement of the dynamic displacement of railway bridges using an advanced video-based system,” *Engineering Structures*, vol. 75, pp. 164–180, 2014. <https://doi.org/10.1016/j.engstruct.2014.04.051> ↑3
- [13] D. Béréziat and I. Herlin, “Motion and acceleration from image assimilation with evolution models,” *Digital Signal Processing*, vol. 83, pp. 45–58, 2018. <https://doi.org/10.1016/j.dsp.2018.08.008> ↑4, 9
- [14] A. Y. Sun, D. Wang, and X. Xu, “Monthly streamflow forecasting using gaussian process regression,” *Journal of Hydrology*, vol. 511, pp. 72–81, 2014. <https://doi.org/10.1016/j.jhydrol.2014.01.023> ↑4

- [15] S. Chatterjee and A. S. Hadi, *Sensitivity analysis in linear regression*. John Wiley Sons, 2009, vol. 327. ↑4
- [16] A. Girard, C. Rasmussen, J. Q. Candela, and R. Murray-Smith, "Gaussian process priors with uncertain inputs application to multiple-step ahead time series forecasting," *Advances in neural information processing systems*, vol. 15, pp. 545–552, 2002. ↑4
- [17] C. E. Rasmussen, "Gaussian processes in machine learning," *Summer School on Machine Learning*, pp. 63–71, 2003. https://doi.org/10.1007/978-3-540-28650-9_4 ↑4
- [18] D. Anguita, A. Ghio, N. Greco, L. Oneto, and S. Ridella, "Model selection for support vector machines: Advantages and disadvantages of the machine learning theory," in *The 2010 international joint conference on neural networks (IJCNN)*, IEEE, 2010, pp. 1–8. <https://doi.org/10.1109/IJCNN.2010.5596450> ↑4
- [19] T. Chan and J. Shen, *Image processing and analysis*. Society for Industrial and Applied Mathematics SIAM, 2005, vol. 94. ↑4, 6
- [20] H. Lin and K. Li, "Motion blur removal and its application to vehicle speed detection," *Electrical Engineering*, no. 2, pp. 3407–3410, 2004. ↑4, 6, 7
- [21] S. Som, "Analysis of the effect of linear smear on photographic images," *JOSA*, vol. 61, no. 7, pp. 859–864, 1971. <https://doi.org/10.1364/JOSA.61.000859> ↑4
- [22] X. Y. Qi, L. Zhang, and C. L. Tan, "Motion deblurring for optical character recognition," in *Document Analysis and Recognition, 2005. Proceedings. Eighth International Conference on*, IEEE, 2005, pp. 389–393. ↑5
- [23] Y. Yitzhaky and A. Stern, "Restoration of interlaced images degraded by variable velocity motion," *Optical Engineering*, vol. 42, no. 12, pp. 3557–3565, 2003. <https://doi.org/10.1117/1.1621406> ↑5
- [24] Y. Yitzhaky, I. Mor, A. Lantzman, and N. Kopeika, "Direct method for restoration of motion-blurred images," *Journal of the Optical Society of America*, vol. 15, no. 6, pp. 1512–1519, 1998. <https://doi.org/10.1364/JOSAA.15.001512> ↑5
- [25] M. Cannon, "Blind deconvolution of spatially invariant image blurs with phase," *Acoustics, Speech and Signal Processing, IEEE Transactions on*, vol. 24, no. 1, pp. 58–63, 1976. <https://doi.org/10.1109/TASSP.1976.1162770> ↑5
- [26] M. Sakano, N. Suetake, and E. Uchino, "Robust identification of motion blur parameters by using angles of gradient vectors," in *Intelligent Signal Processing and Communications, 2006. ISPACS'06. International Symposium on*, IEEE, 2006, pp. 522–525. <https://doi.org/10.1109/ISPACS.2006.364711> ↑5
- [27] M. E. Moghaddam and M. Jamzad, "Linear motion blur parameter estimation in noisy images using fuzzy sets and power spectrum," *EUR-ASIP Journal on Advances in Signal Processing*, vol. 2007, no. 1, pp. 1–8, 2007. <https://doi.org/10.1155/2007/68985> ↑5
- [28] M. A. Lata, S. Ghosh, F. Bobi, and M. A. Yousuf, "Novel method to assess motion blur kernel parameters and comparative study of restoration techniques using different image layouts," in *2016 5th International Conference on Informatics, Electronics and Vision (ICIEV)*, IEEE, 2016, pp. 367–372. <https://doi.org/10.1109/ICIEV.2016.7760027> ↑5

- [29] H.-Y. Lin, "Vehicle speed detection and identification from a single motion blurred image," in *Application of Computer Vision, 2005. WACV/MOTIONS'05 Volume 1. Seventh IEEE Workshops on*, IEEE, vol. 1, 2005, pp. 461–467. ↑7
- [30] M. Celestino and O. Horikawa, "Velocity measurement based on image blur," *Computer graphics and image processing*, vol. 3, pp. 633–642, 2008. ↑7
- [31] H. Pazhoumand-Dar, A. M. T. Abolhassani, and E. Saeedi, "Object speed estimation by using fuzzy set," *World Academy of Science, Engineering and Technology, International Journal of Computer, Electrical, Automation, Control and Information Engineering*, vol. 4, no. 4, pp. 688–691, 2010. ↑7
- [32] S. Rezvankhah, A. A. Bagherzadeh, H. Moradi, and B. N. A. Member, "A Real-time Velocity Estimation using Motion Blur in Air Hockey," in *2012 IEEE International Conference on Robotics and Biomimetics (ROBIO)*, 2012, pp. 1767–1772, <https://doi.org/10.1109/RO-BIO.2012.6491223> ↑7
- [33] J. Mohammadi and A. Taherkhani, "Object Speed Estimation in Frequency Domain of Single Taken Image," *Journal of Basic and Applied Scientific Research*, vol. 3, pp. 120–124, 2013. ↑7
- [34] S. McCloskey, Y. Ding, and J. Yu, "Design and estimation of coded exposure point spread functions," *IEEE transactions on pattern analysis and machine intelligence*, vol. 34, no. 10, p. 2071, 2012. <https://doi.org/10.1109/TPAMI.2012.108> ↑7
- [35] A. Agrawal, Y. Xu, and R. Raskar, "Invertible motion blur in video," in *ACM Transactions on Graphics (TOG)*, vol. 28, 2009, p. 95. <https://doi.org/10.1145/1531326.1531401> ↑7
- [36] M. Lee, K.-S. Kim, and S. Kim, "Measuring vehicle velocity in real time using modulated motion blur of camera image data," *IEEE Transactions on Vehicular Technology*, vol. 66, no. 5, pp. 3659–3673, 2016. <https://doi.org/10.1109/TVT.2016.2600281> ↑7
- [37] M. Lee, "A study on measuring vehicle velocity in real time using modulated motion blur of camera image data," Ph.D. dissertation, Korea Advanced Institute of Science and Technology, 2017. <https://doi.org/10.1109/TVT.2016.2600281> ↑7
- [38] M. Lee, K.-S. Kim, J. Cho, and S. Kim, "Development of a vehicle body velocity sensor using modulated motion blur," in *2017 IEEE International Conference on Advanced Intelligent Mechatronics (AIM)*, IEEE, 2017, pp. 406–411. <https://doi.org/10.1109/AIM.2017.8014051> ↑7
- [39] J. Jing, F. Xiao, L. Yang, S. Wang, and B. Yu, "Measurements of velocity field and diameter distribution of particles in multiphase flow based on trajectory imaging," *Flow Measurement and Instrumentation*, vol. 59, pp. 103–113, 2018. <https://doi.org/10.1016/j.flow-measinst.2017.12.005> ↑7
- [40] K. Matsuo and T. Yakoh, "Position and velocity measurement method from a single image using modulated illumination," in *2018 IEEE 15th International Workshop on Advanced Motion Control (AMC)*, IEEE, 2018, pp. 353–359. <https://doi.org/10.1109/AMC.2019.8371117> ↑7
- [41] J. A. Dwicahya, N. Ramadijanti, and A. Basuki, "Moving object velocity detection based on motion blur on photos using gray level," in *2018 International Electronics Symposium on Knowledge Creation and Intelligent Computing (IES-KCIC)*, IEEE, 2018, pp. 192–198. <https://doi.org/10.1109/KCIC.2018.8628598> ↑

- [42] J. A. Cortes-Osorio, J. B. Gomez-Mendoza, and J. C. Riano-Rojas, "Velocity estimation from a single linear motion blurred image using discrete cosine transform," *IEEE Transactions on Instrumentation and Measurement*, vol. 68, no. 10, pp. 4038–4050, 2019. <https://doi.org/10.1109/TIM.2018.2882261> ↑8, 14, 15
- [43] J. A. Cortes-Osorio, "A contribution to the estimation of kinematic quantities from linear motion blurred images," Ph.D. dissertation, Universidad Nacional de Colombia Sede Manizales, 2020. ↑8, 12
- [44] Q. Guo et al., "Learning to Adversarially Blur Visual Object Tracking," in *Proceedings of the IEEE/CVF International Conference on Computer Vision*, 2021. <https://doi.org/10.1109/ICCV48922.2021.01066> ↑8
- [45] M. Li, H. Du, Q. Zhang, and J. Wang, "Improved particle image velocimetry through cell segmentation and competitive survival," *IEEE Transactions on Instrumentation and Measurement*, vol. 57, no. 6, pp. 1221–1229, 2008. <https://doi.org/10.1109/TIM.2007.915443> ↑8, 20
- [46] X. Liu and J. Katz, "Instantaneous pressure and material acceleration measurements using a four-exposure piv system," *Experiments in Fluids*, vol. 41, no. 2, p. 227, 2006. <https://doi.org/10.1007/s00348-006-0152-7> ↑9, 20
- [47] H. Zhou, M. Chen, L. Zhang, N. Ye, and C. Tao, "Measuring shape and motion of a high-speed object with designed features from motion blurred images," *Measurement*, vol. 145, pp. 559–567, 2019. <https://doi.org/10.1016/j.measurement.2019.05.023> ↑9
- [48] L. Li, T. Martin, and X. Xu, "A novel vision-based real-time method for evaluating postural risk factors associated with musculoskeletal disorders," *Appl. Ergon.*, vol. 87, p. 103 138, 2020. <https://doi.org/10.1016/j.apergo.2020.103138> ↑9
- [49] C. Yu, X. Bi, and Y. Fan, "Deep learning for fluid velocity field estimation: A review," *Ocean Engineering*, vol. 271, p. 113 693, 2023. <https://doi.org/10.1016/j.oceaneng.2023.113693> ↑9
- [50] P. Chu, B. T. Wolfe, and Z. Wang, "Measurement of incandescent microparticle acceleration using stereoscopic imaging," *Review of Scientific Instruments*, vol. 89, no. 10, 2018. <https://doi.org/10.1063/1.5034311> ↑10
- [51] G. Chen, L. Li, C. Zhao, R. Huang, and F. Guo, "Acceleration characteristics of a rockslide using the particle image velocimetry technique," *Journal of Sensors*, vol. 2016, 2016. <https://doi.org/10.1155/2016/2650871> ↑10
- [52] D. C. Luvizon, B. T. Nassu, and R. Minetto, "A video-based system for vehicle speed measurement in urban roadways," *IEEE Transactions on Intelligent Transportation Systems*, vol. 18, no. 6, pp. 1393–1404, 2017. <https://doi.org/10.1109/TITS.2016.2600281> ↑10
- [53] J. X. Wang, "Research of vehicle speed detection algorithm in video surveillance," in *Audio, Language and Image Processing (ICALIP), 2016 International Conference on*, IEEE, 2016, pp. 349–352. <https://doi.org/10.1109/ICALIP.2016.7846482> ↑10
- [54] K. V. K. Kumar, P. Chandrakant, S. Kumar, and K. J. Kushal, "Vehicle speed detection using corner detection," in *2014 Fifth International Conference on Signal and Image Processing*, 2014, pp. 253–258. <https://doi.org/10.1109/ICSIP.2014.46> ↑10

- [55] J. Dong, Y. Song, H. Wang, J. Zeng, and Z. Wu, "Predicting flow velocity affected by seaweed resistance using svm regression," in *Computer Application and System Modeling (ICCASM), 2010 International Conference on*, vol. 2, 2010, pp. V2–273. <https://doi.org/10.1109/IC-CASM.2010.5620588> ↑10
- [56] O. Genç and A. Dağ, "A machine learning-based approach to predict the velocity profiles in small streams," *Water Resources Management*, vol. 30, no. 1, pp. 43–61, 2016. <https://doi.org/10.1007/s11269-015-1123-7> ↑10
- [57] M. Morimoto, K. Fukami, and K. Fukagata, "Experimental velocity data estimation for imperfect particle images using machine learning," *arXiv preprint arXiv:2005.00756*, 2020. <https://doi.org/10.1063/5.0060760> ↑10
- [58] P. J. Chun, T. Yamane, S. Izumi, and N. Kuramoto, "Development of a machine learning-based damage identification method using multipoint simultaneous acceleration measurement results," *Sensors*, vol. 20, no. 10, p. 2780, 2020. <https://doi.org/10.3390/s20102780> ↑10
- [59] W. Kim, M. Tanaka, M. Okutomi, and Y. Sasaki, "Learning-based human segmentation and velocity estimation using automatic labeled lidar sequence for training," *IEEE Access*, vol. 8, pp. 88 443–88 452, 2020. <https://doi.org/10.1109/ACCESS.2020.2993299> ↑10
- [60] B. Major, D. Fontijne, A. Ansari, et al., "Vehicle detection with automotive radar using deep learning on range-azimuth-doppler tensors," in *2019 IEEE/CVF International Conference on Computer Vision Workshop (ICCVW)*, 2019, pp. 924–932. <https://doi.org/10.1109/ICCVW.2019.00121> ↑10
- [61] C. Guo, Y. Fan, C. Yu, Y. Han, and X. Bi, "Time-resolved particle image velocimetry algorithm based on deep learning," *IEEE Transactions on Instrumentation and Measurement*, vol. 71, pp. 1–13, 2022. <https://doi.org/10.1109/TIM.2022.3141750> ↑10
- [62] S. Cai, J. Liang, Q. Gao, C. Xu, and R. Wei, "Particle image velocimetry based on a deep learning motion estimator," *IEEE Transactions on Instrumentation and Measurement*, vol. 69, no. 6, pp. 3538–3554, 2020. <https://doi.org/10.1109/TIM.2019.2932649> ↑10
- [63] A. Oppenheim, R. Schafer, and T. Stockham, "Nonlinear filtering of multiplied and convolved signals," *IEEE Transactions on Audio and Electroacoustics*, vol. 16, no. 3, pp. 437–466, 1968. <https://doi.org/10.1109/TAU.1968.1161990> ↑12
- [64] I. Pitas and A. N. Venetsanopoulos, "Homomorphic Filters," in *Nonlinear Digital Filters: Principles and Applications*, Springer US, 1990, pp. 217–243. https://doi.org/10.1007/978-1-4757-6017-0_7 ↑12
- [65] T. M. Cannon, "Digital image deblurring by nonlinear homomorphic filtering," Utah University, Salt Lake City School of Computing, Tech. Rep., 1974. <https://doi.org/10.21236/ADA002735> ↑12, 13
- [66] Y. Yitzhaky, R. Milberg, S. Yohaev, and N. S. Kopeika, "Comparison of direct blind deconvolution methods for motion-blurred images," *Applied Optics*, vol. 38, no. 20, pp. 4325–4332, 1999. <https://doi.org/10.1364/AO.38.004325> ↑12
- [67] J. A. Cortes-Osorio, D. A. Muñoz-Acosta, and C. D. López-Robayo, "Design and construction of an electromechanical slider for the kinematic study of linear motion blurred images," *INGE CUC*, vol. 16, no. 1, pp. 80–90, 2020. <https://doi.org/10.17981/ingecuc.16.1.2020.06> ↑15, 17

- [68] Basler, *aca2000-165um-baslerace*, <https://www.baslerweb.com/en/products/cameras/area-scan-cameras/ace/aca2000-165um/>, (Accessed on 06/11/2017), Nov. 2017. ↑15
- [69] Ricoh *lens fl-cc0814a-2m*, <https://www.baslerweb.com/en/products/vision-components/lenses/ricoh-lens-fl-cc0814a-2m-fl-4-f8mm-2-3/>, (Accessed on 06/11/2017), Nov. 2017. ↑15
- [70] *BT.601: Studio encoding parameters of digital television for standard 4:3 and wide screen 16:9 aspect ratios*, <http://www.itu.int/rec/rrec-bt.601>, 2017. ↑15
- [71] E. Izquierdo-Verdiguier, L. Gomez-Chova, L. Bruzzone, and G. Camps-Valls, "Semisupervised kernel feature extraction for remote sensing image analysis," *IEEE Transactions on Geoscience and Remote Sensing*, vol. 52, no. 9, pp. 5567–5578, 2014. <https://doi.org/10.1109/TGRS.2013.2290372> ↑15
- [72] T. Bouwmans, S. Javed, H. Zhang, Z. Lin, and R. Otazo, "On the applications of robust PCA in image and video processing," *Proceedings of the IEEE*, vol. 106, no. 8, pp. 1427–1457, 2018. <https://doi.org/10.1109/JPROC.2018.2853589> ↑16
- [73] P. S. GmbH, *Cobra4 sensor unit 3D acceleration*, <https://repository.curriculab.net/files/bedan1.pdf/12650.00/1265000e.pdf>, 2018. ↑17
- [74] L. Kirkup and R. B. Frenkel, *An introduction to uncertainty in measurement: using the GUM (guide to the expression of uncertainty in measurement)*. Cambridge University Press, 2006. <https://doi.org/10.1017/CBO9780511755538> ↑17
- [75] R. H. Dieck, *Measurement uncertainty: methods and applications*. ISA, 2007. ↑17
- [76] A. J. Sederman, M. D. Mantle, C. Buckley, and L. F. Gladden, "MRI technique for measurement of velocity vectors, acceleration, and auto-correlation functions in turbulent flow," *Journal of Magnetic Resonance*, vol. 166, no. 2, pp. 182–189, 2004. <https://doi.org/10.1016/j.jmr.2003.10.016> ↑20
- [77] K. Komiya, T. Kurihara, and S. Ando, "3D particle image velocimetry using correlation image sensor," in *Proc. SICE Annual Conf.* 2011, Sep. 2011, pp. 2774–2778. ↑20

Jimmy Alexander Cortés-Osorio

JA Cortés-Osorio is an accomplished academic who has significantly contributed to engineering and physics. Born in Pereira, Colombia. He obtained a BE in Electrical Engineering and an MS in Physics Instrumentation from Universidad Tecnológica de Pereira (UTP) in 1999 and 2009, respectively. In 2020, he received a PhD in Automatic Engineering from Universidad Nacional de Colombia, Manizales campus. Since 2013, Cortés-Osorio has served as a full professor of the Departments of Physics and Engineering at UTP. He has conducted research in various fields of engineering, including image processing, image motion analysis, machine vision, machine learning, data mining, and instrumentation and measurement. His current research interests are focused on these areas, and he has made significant contributions to the field through his research and publications. Cortés-Osorio is an affiliate member of the Society for Industrial and Applied Mathematics (SIAM) and the Institute of Electrical and Electronic Engineers (IEEE). Additionally, he has served in various academic committees, including

UTP's research committee and the academic council, where he has contributed to developing academic programs and research initiatives.

Email: jacoper@utp.edu.co

Juan Bernardo Gómez-Mendoza

J.B. Gómez-Mendoza obtained his bachelor's degree in electronic engineering, a master's degree in industrial Automation, and a Doctoral degree in Engineering – Automation from Universidad Nacional de Colombia in 2002, 2004, and 2012, respectively. He has been attached to the Department of Electrical, Electronic, and Computer Engineering of Universidad Nacional de Colombia at Manizales since February 2005, currently holding the position of associate professor. His areas of interest include image processing, machine vision, artificial intelligence and data analysis, and robotics.

Email: jbgomezm@unal.edu.co

Juan Carlos Riaño-Rojas

JC Riano-Rojas is an academic who has contributed significantly to mathematics in Manizales. He was born in Bogotá, Colombia. He obtained a bachelor's and a master's degree in mathematical sciences from Universidad Nacional de Colombia in 1992 and 1998, respectively. In 2013, he received a PhD in Automatic Engineering, and, in 2020, he received a Specialist's degree in Statistics from Universidad Nacional de Colombia, Manizales campus. Since 1999, Riano-Rojas has served as an associate professor of the Department of Mathematics and Statistics of Universidad Nacional de Colombia. He has conducted research in various fields of mathematics and engineering, including image processing, image motion analysis, computer vision, machine learning, topology, mathematical logic, and data sciences. His current research interests focus on these areas, and he has made significant contributions to the field through his research and publications.

Email: jcrianoro@unal.edu.co

